Supplementary Online Material to:

Membrane protein sequestering by ionic protein-lipid interactions

Geert van den Bogaart[1], Karsten Meyenberg[2], H. Jelger Risselada[3], Hayder Amin[1], Katrin I. Willig[4], Barbara E. Hubrich[2], Markus Dier[1], Stefan W. Hell[4], Helmut Grubmüller[3], Ulf Diederichsen[2], Reinhard Jahn[1]

1- Department of Neurobiology, Max Planck Institute for Biophysical Chemistry, Am Faßberg 11, 37077, Göttingen, Germany

2- Institute for Organic and Biomolecular Chemistry, Georg-August-University Göttingen, Tammannstraße 2, 37077, Göttingen, Germany

3- Department of Theoretical and Computational Biophysics, Max Planck Institute for Biophysical Chemistry, Am Faßberg 11, 37077, Göttingen, Germany

4- Department of Nanobiophotonics, Max Planck Institute for Biophysical Chemistry, Am Faßberg 11, 37077, Göttingen, Germany

Correspondence should be addressed to R.J. (R.Jahn@gwdg.de)

Supplementary Methods

PH_{PLCδ}-citrine purification

For the PH_{PLCδ}-citrine reporter, a synthetic gene (Genscript; sequence below) was inserted into the NdeI − EcoRI restriction sites of pET-28a(+). This gene codes for residues 1–170 of human 1-phosphatidylinositol-4,5-bisphosphate phosphodiesterase delta-1 (PLCδ1; Swiss-Prot P51178)[30] fused *N*-terminally to citrine, a monomeric YFP analog[10]. The codon usage was optimized for expression in *Escherichia coli* (strain K12).

Expression of PH_{PLCδ}-citrine was induced in exponential growing *E. coli* BL21(DE3) with 0.5 mM IPTG for 3 h. The protein was subsequently purified with conventional his-tag affinity purification. Briefly, the cells where first harvested by centrifugation for 30 min at 3,200 ×g. The pellet was then resuspended in ~5 volumes (wet pellet) of 20 mM Hepes pH 7.4, 500 mM NaCl and 8 mM imidazole supplemented with 1 mg/ml lysozyme, 1 mM PMSF, 1 mM MgSO_4 and a spatula tip of DNaseI. This cell suspension was then incubated for 30 min at room temperature. Subsequently, 5% (m/w) cholate was added, followed by an additional 45 min incubation step. The cells where ruptured by ultrasonication and the intact cells and cell membranes were removed by 20 min centrifugation at 34,000 ×g. The supernatant was incubated with 5% (v/v) nickel-sepharose beads under gentle shaking at 4°C for 3 h. The beads were drained and washed with 300 column volumes of 20 mM Hepes pH 7.4, 500 mM NaCl, 10% (w/v) glycerol, and 20 mM imidazole. Afterward, the protein was eluted with the same buffer, but now with 400 mM imidazole. The his-tag was removed by an overnight incubation at 4°C with 100 U thrombin. The protein was stored at 4°C, as flash freezing in liquid N_2 and subsequent thawing led to aggregation of the protein. In addition, the protein was used within one week after purification as it deteriorated in time.

Sequence of PH_{PLCδ}-citrine:

```
CATATGGACT CTGGTCGTGA CTTCCTGACC CTGCACGGTC TGCAGGACGA CGAAGACCTG
CAGGCTCTGC TGAAAGGTTC TCAGCTGCTG AAAGTTAAAT CTTCTTCTTG GCGTCGTGAA
CGTTTCTACA AACTGCAGGA AGACTGCAAA ACCATCTGGC AGGAATCTCG TAAAGTTATG
CGTACCCCGG AATCTCAGCT GTTCTCTATC GAAGACATCC AGGAAGTTCG TATGGGTCAC
CGTACCGAAG GTCTGGAAAA ATTCGCTCGT GACGTTCCGG AAGACCGTTG CTTCTCTATC
GTTTTCAAAG ACCAGCGTAA CACCCTGGAC CTGATCGCTC CGTCTCCGGC TGACGCTCAG
CACTGGGTTC TGGGTCTGCA CAAAATCATC CACCACTCTG TTCTATGGA CCAGCGTCAG
AAACTGCAGC ACTGGATCCA CTCTTGCCTG CGTAAAGCTG ACAAAAACAA AGACAACAAA
ATGTCTTTCA AGAACTGCA GAACTTCCTG AAAGACCCGC CGGTTGCTAC TATGGTTTCT
AAAGGTGAAG AACTGTTCAC CGGTGTTGTT CCGATCCTGG TTGAACTGGA CGGTGACGTT
AACGGTCACA AATTCTCTGT TTCTGGTGAA GGTGAAGGTG ACGCTACCTA CGGTAAACTG
ACCCTGAAAT TCATCTGCAC CACCGGTAAA CTGCCGGTTC CGTGGCCGAC CCTGGTTACC
ACCTTCGGTT ACGGTCTGAT GTGCTTCGCT CGTTACCCGG ACCACATGAA ACAGCACGAC
TTCTTCAAAT CTGCTATGCC GGAAGGTTAC GTTCAGGAAC GTACCATCTT CTTCAAAGAC
GACGGTAACT ACAAAACCCG TGCTGAAGTT AAATTCGAAG GTGACACCCT GGTTAACCGT
```

```
ATCGAACTGA AAGGTATCGA CTTCAAAGAA GACGGTAACA TCCTGGGTCA CAAACTGGAA
TACAACTACA ACTCTCACAA CGTTTACATC ATGGCTGACA AACAGAAAAA CGGTATCAAA
GTTAACTTCA AAATCCGTCA CAACATCGAA GACGGTTCTG TTCAGCTGGC TGACCACTAC
CAGCAGAACA CCCCGATCGG TGACGGTCCG GTTCTGCTGC CGGACAACCA CTACCTGTCT
TACCAGTCTG CTCTGTCTAA AGACCCGAAC GAAAACGTG ACCACATGGT TCTGCTGGAA
TTTGTTACCG CTGCTGGTAT CACCCTGGGT ATGGACGAAC TGTACAAATA ATAAGAATTC
```

Syntaxin-1A$_{259-288}$-GFP reporters

For the GFP-syntaxin-1A reporters, we used syntaxin-1A (residues 1–28 + 259–288) linked to GFP (Supp. Fig. 10–11)[24]. This peptide contains both the transmembrane helix and the polybasic juxtamembrane region of syntaxin-1A. It is *C*-terminally attached via a 12 residue linker (LVPRARDPPVAT) to a monomeric version of enhanced GFP (meGFP)[24]. The synthetic genes (Genscript; sequence below; see also reference (24)) were ordered in the KpnI – HindIII restriction sites of pCEP4 (Invitrogen). Codon usage was optimized for expression in mouse.

Sequences of the GFP-reporters:

With wild-type linker region (KARRKK):

```
GGTACCATGA AGGACAGGAC CCAGGAGCTG AGGACCGCCA AGGACAGCGA CGACGACGAC
GACGTGACCG TGACCGTGGA CAGGGACAGG AGCAAGGCCA GGAGGAAGAA GATCATGATC
ATCATCTGCT GCGTGATCCT GGGCATCATC ATCGCCAGCA CCATCGGCGG CATCTTCGGC
CTGGTGCCCA GGGCCAGGGA CCCCCCCGTG GCCACCATGG TGAGCAAGGG CGAGGAGCTG
TTCACCGGCG TGGTGCCCAT CCTGGTGGAG CTGGACGGCG ACGTGAACGG CCACAAGTTC
AGCGTGAGCG GCGAGGGCGA GGGCGACGCC ACCTACGGCA AGCTGACCCT GAAGTTCATC
TGCACCACCG GCAAGCTGCC CGTGCCCTGG CCCACCCTGG TGACCACCCT GACCTACGGC
GTGCAGTGCT TCAGCAGGTA TCCCGACCAC ATGAAGCAGC ACGACTTCTT CAAGAGCGCC
ATGCCCGAGG GCTACGTGCA GGAGAGGACC ATCTTCTTCA AGGACGACGG CAACTACAAG
ACCAGGGCCG AGGTGAAGTT CGAGGGCGAC ACCCTGGTGA ACAGGATCGA GCTGAAGGGC
ATCGACTTCA AGGAGGACGG CAACATCCTG GGCCACAAGC TGGAGTACAA CTACAACAGC
CACAACGTGT ACATCATGGC CGACAAGCAG AAGAACGGCA TCAAGGTGAA CTTCAAGATC
AGGCACAACA TCGAGGACGG CAGCGTGCAG CTGGCCGACC ACTACCAGCA GAACACCCCC
ATCGGCGACG GCCCCGTGCT GCTGCCCGAC AACCACTACC TGAGCACCCA GAGCAAGCTG
AGCAAGGACC CCAACGAGAA GAGGGACCAC ATGGTGCTGC TGGAGTTCGT GACCGCCGCC
GGCATCACCC TGGGCATGGA CGAGCTGTAC AAGTAGTAGA AGCTT
```

K264A mutant (KARRAK):
Same as above, but with the underlined bases converted to: GCCAAG
K264A K265A mutant (KARRAA):
Same as above, but with the underlined bases converted to: GCCGCG

Cell culture and immunofluorescence

PC12 cells were maintained and propagated as described[3,24]. PC12 cells were transfected using the Lipofectamine LTX reagents and protocol from Invitrogen. Experiments with PC12 cells were carried out 24 hours posttransfection. Membrane sheets were prepared by rupturing the cells with probe sonication as described[24]. Immunostaining was performed as described[24]. For detection of syntaxin-1A, we used the monoclonal antibody HPC-1[31] and a polyclonal antibody from rabbit (raised against syntaxin-1A residues 183–240). PIP2 was immunostained with a monoclonal antibody (IgM; 2C11; Abcam, catalogue nr. ab11039). For immunofluorescence, we applied immunoglobulins G labeled with DyLight 649 (Dianova, catalogue nr. 115-495-072), Cy3 (Dianova, 115-165-072) and Alexa Fluor 488 (Invitrogen, A10680) and a Cy5-labeled F(ab')$_2$-fragment (Dianova, 111-176-144). PH$_{PLC\delta}$-citrine (1.2 µM in PBS) labeling of the membrane sheets was performed by 20 minutes incubation at room temperature, followed by extensive washing with PBS.

Fluorescence microscopy

Membrane sheets were imaged by epi-fluorescence in PBS containing 2 µM 1-(4-trimethylammoniumphenyl)-6-phenyl-1,3,5-hexatriene (TMA-DPH; Invitrogen)[32] as described[24]. STED microscopy was performed as described[33,34]. TIRF microscopy was measured on a homebuilt setup based on an Axiovert 200 microscope body (Zeiss) fitted with a Plan-FLUAR 100× 1.45 NA objective. The 488 nm line of a 500 mW multiline argon ion laser (LGK7880ML, National Laser) was used for excitation of the GFP and emission was collected with a back-illuminated EM-CCD (DU-897E, Andor).

Supported bilayers spin-coating

50 µl of a 1 mg/ml lipid solution in chloroform was spin coated at 2,500 rpm on a 18 mm diameter coverslip. The spin coater was constructed from a CPU cooler[35] and had a constant velocity of 2,500 rpm. This procedure yields highly oriented and homogenous single bilayers[36]. These bilayers were stained with PH$_{PLC\delta}$-citrine as described for the membrane sheets.

Peptide synthesis

The peptides were synthesized via Fmoc solid phase synthesis on preloaded Fmoc-Gly Wang resin LL (low loading; 0.3 mmol g^{-1}). Chain elongation was performed on the microwave assisted automatic peptide synthesizer Liberty with an additional module of Discover (CEM Corporation) that provides microwave energy at 2,450 MHz. Fmoc deprotection was performed with 20% piperidine in NMP. Fmoc amino acids were prepared as 0.2 M solutions in NMP. Coupling reactions were performed as double coupling with 0.5 M HBTU/HOBt (5 equiv.) in DMF, 0.2 M amino acids in NMP (5 equiv.) and with 2 M DIPEA (10 equiv.) in NMP. Capping has been done for every cycle using a solution of acetic anhydrid (10%), DIPEA (5%) and HOBt (0.2%) in NMP. Deprotection, coupling and capping reactions were performed with microwave energy and N$_2$ mixing. A deprotection microwave cycle was characterized by two deprotection steps of 30 and 180 s, respectively. All microwave coupling reactions except for arginine were performed for 300 s at 75ºC. Arginine has been coupled under N$_2$

mixing for 1,500 s at room temperature followed by microwave assisted coupling for 300 s at 50°C. Standard Fmoc amino acid building blocks have been used for the peptide syntheses.

For the preparation of fluorescently labeled peptides, the fluorescent dye Atto647N NHS-ester (Atto-Tec) was coupled *N*-terminally to the peptides on solid support using an excess of dye (5 molar equiv.) and DIPEA (10 equiv.) at room temperature for 12 hours. Rhodamine red succinimidyl ester (Invitrogen) was coupled in the same manner. After coupling of the dye, the resin was washed thoroughly with DCM and diethylether and dried in a high vacuum over night. Cleavage from the solid support was carried out with a mixture of TFA, water, EDT and TES (94 : 2.5 : 2.5 : 1 volume ratio, 10 ml g^{-1} resin) for 2 h. The resin was filtered off and the solution was concentrated by flushing with N_2. The peptides were precipitated from cold MTBE, centrifuged and lyophilized. Prior to coupling of the fluorescence dye, the integrity of the peptide was confirmed by ESI-MS. The transmembrane peptides were difficult to purify. Analysis with HPLC-MS using a C4-column showed an elution of peptide molecule ions over the whole run time, probably due to peak broadening caused by aggregation of the peptides. Consequently, the peptides were used directly after lyophilisation without chromatographic purification. We believe this is justified, because: (*i*) mass spectrometry showed only little fragmentation. (*ii*) It has been reported that similar transmembrane peptides behave identical to purified peptides[37]. (*iii*) Most importantly, only complete peptides (and not incomplete intermediates) are fluorescently labeled, because the fluorophore is only coupled to fully protected peptide.

All peptides were verified by electrospray ionization mass spectroscopy ESI-MS and/or high resolution MS (HR-MS). Spectra were optained using a Bruker Apex-Q IV 7T or a Bruker micrOTOF. Atto647N-syntaxin-1A$_{257-288}$ wild type; Atto647N− YQSKA RRKKI MIIIC CVILG IIIAS TIGGI FG −OH; $C_{201}H_{325}N_{45}O_{40}S_3$, mass 4,105.4; ESI-MS, m/z: 1,127.85 [M+4H]$^{4+}$; HR-MS: calculated [M+4H]$^{4+}$ 1127.8572, found 1,127.8548. Atto647N-syntaxin-1A$_{257-288}$ K264A; Atto647N− YQSKA RRAKI MIIIC CVILG IIIAS TIGGI FG −OH; $C_{198}H_{319}N_{44}O_{40}S_3$, mass 4,049.3; ESI-MS, m/z (%): 811.08 (17) [M+3H]$^{3+}$, 1,013.59 (100) [M+4H]$^{4+}$; HR-MS: calculated [M+4H]$^{4+}$ 810.6744, found 810.6746. Atto647N-syntaxin-1A$_{257-288}$ K264A K265A; Atto647N− YQSKA RRAAI MIIIC CVILG IIIAS TIGGI FG −OH; $C_{195}H_{312}N_{43}O_{40}S_3$, mass 3,992.3; ESI-MS, m/z: 999.58 [M+4H]$^{4+}$, 1,332.44 [M+4H]$^{3+}$; HR-MS: calculated [M+3H]$^{3+}$ 1,331.4322, found 1,331.4335. Atto647N-syntaxin-1A$_{257-288}$ M267A C271A I279A; Atto647N− YQSKA RRKKI AIIIA CVILG IIAAS TIGGI FG –OH; $C_{196}H_{315}N_{45}O_{40}S$; mass 3,974.95; ESI-MS, m/z: 3,974.95; HR-MS: calculated [M+4H]$^{4+}$ 993.8502, found 993.8505. Rhodamine red-syntaxin-1A$_{257-288}$ wild type; rhodamine red− YQSKA RRKKI MIIIC CVILG IIIAS TIGGI FG −OH; $C_{192}H_{315}N_{45}O_{45}S_5$, mass 4,131.2; ESI-MS, m/z: 4,132.2 [M+H]$^+$.

Reconstitution into GUVs
DOPC, DOPS (1,2-dioleoyl-sn-glycero-3-phosphatidylcholine and –serine), cholesterol, brain PIP2 and dioleoyl-PiP2 (1,2-dioleoyl-sn-glycero-3-phosphatidyl-(1'-myo-inositol-4',5'-bisphosphate)) were from Avanti Polar Lipids. Bodipy-labeled PIP2 (bodipy-TMR-PI(4,5)P$_2$,C$_{16}$) was from Echelon Biosciences.

The membranes were labeled with 1.5 mol% of either Oregon green 488-DHPE or DiO (3,3'-dioctadecyloxacarbocyanine; both from Invitrogen). The GUVs were formed by the drying rehydration procedure[38]. For the GUV formation, 1 mg/ml total lipid concentration in ethanol was mixed with 3 mol% of peptide in 2,2,2-trifluoroethanol (TFE). 1 μl of this mixture was then dried on a microscope coverslip for 2 min at 50–60°C, followed by rehydration in 20 mM Hepes pH 7.4.

Laurdan imaging

6-dodecanoyl-2-dimethylaminonaphthalene (Laurdan) was from Sigma. The membranes were stained by adding 0.5–1% (total lipids) Laurdan (in ethanol) after formation of the GUVs[22]. Laurdan was excited by 2-photon microscopy with a Chameleon-Ultra II tunable infrared laser (Coherent) operating at 800 nm. Emission was captured at 400–450 nm (channel 1) and 490–560 (channel 2). To calculate the GP values, calibration measurements were performed with Laurdan in DMSO, as described[22,39]. GP values were then calculated from the images as described[22,39].

Calculation of the PIP2 concentration

We estimated the peak concentration of PIP2 in the microdomains in the PC12 plasma membrane. These microdomains were roughly 73 nm (full width at half maximum; FWHM) as determined by STED microscopy on $PH_{PLC\delta}$-citrine and an antibody raised against PIP2 (Fig. 1). Quantitative imaging using diffraction-limited epi-fluorescence microscopy showed that PIP2 was accumulated at 2.8 ± 0.3% (s.e.m., n = 305) while the background level of PIP2 was 1.2 ± 0.2% (s.e.m., n = 25; Supp. Fig. 2). For the calculation of the PIP2 concentration in the ~73 nm microdomains, we performed the following steps:

1. First, we determined the resolution of the epi-fluorescence microscope used for the quantification of PIP2 in the diffraction limited microdomains (Supp. Fig. 2). 0.2 μm-sized fluorescent beads (Fluorospheres, 505/515; Invitrogen) were imaged with the same microscope. The fluorescent intensity profiles of several beads were then fitted with Gaussian distributions (Supp. Fig. 2f). For the width of the distribution (variance) ω_{epi}, we obtained a value of 445 nm.

2. Second, we calculated the total amount of PIP2 in a 2-dimensional Gaussian distribution with a spread of 445 nm and a peak PIP2 concentration C_{epi} = 2.8 − 1.2 = 1.6% (background subtracted). The black curve in figure 1d shows this distribution.

3. Third, we calculated the peak PIP2 concentration C_{domain} when the total amount of PIP2 (from step 2) was concentrated and Gaussian distributed with a FWHM of 73 nm (the approximate size of the microdomains). Here, we thus assumed that PIP2 is Gaussian distributed over the microdomains.

In total, we approximated the peak concentration of PIP2 in these domains C_{domain} with:

$$\int\limits_{-\infty}^{\infty}\int\limits_{-\infty}^{\infty}\left[C_{epi}\exp\left(-\frac{x^2+y^2}{2\omega_{epi}^2}\right) - C_{domain}\exp\left(-\frac{x^2+y^2}{2\omega_{domain}^2}\right)\right]\mathrm{d}x\,\mathrm{d}y = 0\,,$$

where C_{epi} is the peak concentration of PIP2 in the diffraction limited spots with the background fluorescence subtracted (*i.e.* 2.8 – 1.2 = 1.6%; Supp. Fig 2e). ω_{domain} is the variance of the Gaussian PIP2 distribution in the microdomains, and can be calculated from the FWHM (73 nm, Fig. 1a–c) by a division over $\sqrt{2\ln 2}$, or 62 nm.

A value for C_{domain} of 82% PIP2 was obtained. The distribution of PIP2 in these 73 nm domains is plotted in red in figure 1d. However, this is only a crude estimate as small errors in ω_{domain}, ω_{epi} and C_{epi} will introduce a substantial error. Also, at those high PIP2 concentrations, the fluorescence of the $PH_{PLC\delta}$-citrine reporter is no longer linearly related to the PIP2 concentration due to molecular crowding and/or fluorescence self quenching (Supp. Fig. 2c). Moreover, $PH_{PLC\delta}$-citrine and PIP2-antibody binding (Fig. 1, Supp. Fig. 1) might alter the distribution of PIP2 and are only indicative of PIP2 microdomains but might also be explained by membrane accumulations (such as incompletely removed intracellular material). Lastly, this approximation is based on the assumption that the $PH_{PLC\delta}$-citrine domain binds equally well to PIP2 in the microdomains and to supported bilayers[9]. All these assumptions and uncertainties impair a precise quantification of PIP2 in the microdomains. Nevertheless, the clear punctuate staining in the very small microdomains shows that the $PH_{PLC\delta}$-domain must be highly accumulated, and the local concentration of PIP2 must be very high accordingly. Therefore, we believe that it is safe to conclude that PIP2 is the dominant inner-leaflet lipid at the microdomains.

Molecular dynamics

Simulation model and settings

The molecular dynamics simulations were performed with the GROMACS simulation package[40], version 4.0.7. We used the MARTINI coarse-grained model[25,26,41] to simulate the lipids, amino acids and polar solvents. In our simulations, the orientational polarizability of water is modeled by a three-bead model that represents four water molecules. This substantially reduces the size of the simulation system and enables to study systems that were hitherto considered too large for molecular dynamics simulations[26]. In all simulations, the system was coupled to a constant temperature bath[42] with a relaxation time of 1.0 ps. We performed our simulations at temperatures of both 310 and 350 K and domain formation was observed under both conditions. Periodic boundary conditions where applied to simulate bulk behavior. The time step used in the simulation was 20 fs[43]. Inclusion of (long range) electrostatics interactions are of crucial importance for electrostatic driven protein-lipid clustering. Therefore, we applied the Particle-Mesh Ewald method (PME) to account for long range electrostatic interactions in our simulations. The dielectric constant in the simulations was $\varepsilon_r = 2.5$. The neighbor-list was updated every 10 simulation steps. The pressure was weakly coupled[42] to 1 bar with a relaxation time of 0.5 ps. In analogy to the other studies done with the MARTINI model, the time scales quoted in

this work were scaled by a factor of four to approximately correct for the faster diffusion rates of water and lipids in the coarse-grained model[25].

Modeling syntaxin-1A$_{257-288}$

Syntaxin-1A$_{257-288}$ was modeled using the MARTINI model for proteins, which qualitatively captures the chemical nature of each individual amino acid and includes the secondary structure. The MARTINI model, however, cannot predict secondary structure. Instead, the secondary structure in the protein backbone is already included in the model by restraining the backbone[41]. In our simulations, the transmembrane domain of syntaxin-1A (residues 266–288) was modeled as an α-helix. We assumed first that the intrinsic α-helical linker (partly) unfolds during complex formation with PIP2 and therefore modeled the linker (residues 257–265) as a random coil (Supp. Fig. 14). Secondly, we performed similar simulations, but now with the linker unstructured. In both cases, PIP2 facilitated syntaxin-1A clustering. The *N*-terminal of the simulated syntaxin-1A$_{257-288}$ peptide (Y257) was uncharged to prevent the effect of additional charge.

Modeling phosphoinositides

In our model PIP2 was represented by a coarse-grained mimic able to reproduce the experimentally obtained results. The applied bonded and non-bonded parameters are standard parameters within the MARTINI model[25]. The inositol group in the PIP2 model was included as a triangular ring structure, inspired on a recent parameterized coarse-grained model of glucose[44], and was formed by three weakly polar beads (MARTINI type P2)[25], representing the presence of the three alcohol groups. To each of these three beads a phosphate group (type Qa) was bound with a charge of -2 for the two free phosphate groups and -1 for the glycerol bound phosphate group. The glycerol group was modeled by two intermediate polar beads (type Na). Connected to the glycerol were a stearoylic and an arachidonic acid, which is the predominant PIP2 species in the brain. The saturated stearoylic acid was modeled by four apolar C1 beads, and the poly-unsaturated arachidonic acid by four slightly less apolar C4 beads. Phosphatidylinositol 3-phosphate or PI3P, which results after 5-dephosphorylation of PIP2 (*i.e.* by synaptojanin-1), was modeled by explicitly removing one of the two free phosphate groups from the inositol ring-structure. To mimic the addition of an extra alcohol group after dephosphorylation to the unbound inositol bead, the polarity of this bead was increased (type P2 to P4).

System setup for spontaneous clustering

The simulations used to study spontaneous PIP2-syntaxin-1A$_{257-288}$ clustering contained 64 copies of syntaxin-1A$_{257-288}$ and 40 copies of PIP2 or PI3P, embedded in a 30×30 μm planar bilayer containing 2,520 DOPC lipids and 20,000 solvent molecules. The total charge of the system was kept at zero with Na$^+$ or Cl$^-$ counterions. To mimic the cell membrane, all syntaxin-1A$_{257-288}$ peptides were embedded with their *N*-termini facing the same side of the membrane, and PIP2 or PI3P was only added to the membrane leaflet at the *N*-terminal side. These simulations were run for about 16 μs (Supp. Fig. 15).

Complementary, we also performed 8 μs simulations with smaller 13 × 13 bilayer systems (~500 lipids total) that contained 16 copies of syntaxin-1A$_{257–288}$ and 0–25 copies of PIP2 plus additionally 150 mM NaCl and with or without 20% DOPS. The serine group in DOPS was modeled as a P5 interaction site within the Martini forcefield[25]. We simulated several scenarios (Supp. Fig. 15): (*i*) clustering in pure DOPC bilayers, (*ii*) clustering with PIP2, (*iii*) clustering with PI3P, (*iv*) clustering with PIP2 in the presence of 20% DOPS, (*v*) clustering with PIP2 in the presence of excess Ca^{2+}, (*vi*) clustering with PIP2 and an α-helical instead of an unstructured linker (Supp. Fig. 14), and (*vii*) clustering with PIP2 of syntaxin-1A$_{257–288}$ M267A C271A I279A, that does not homodimerize[23]. In all these simulations, only the absence of PIP2 (*i*) or replacement by PI3P (*iii*) significantly reduced the observed syntaxin-1A clustering (Supp. Fig. 15).
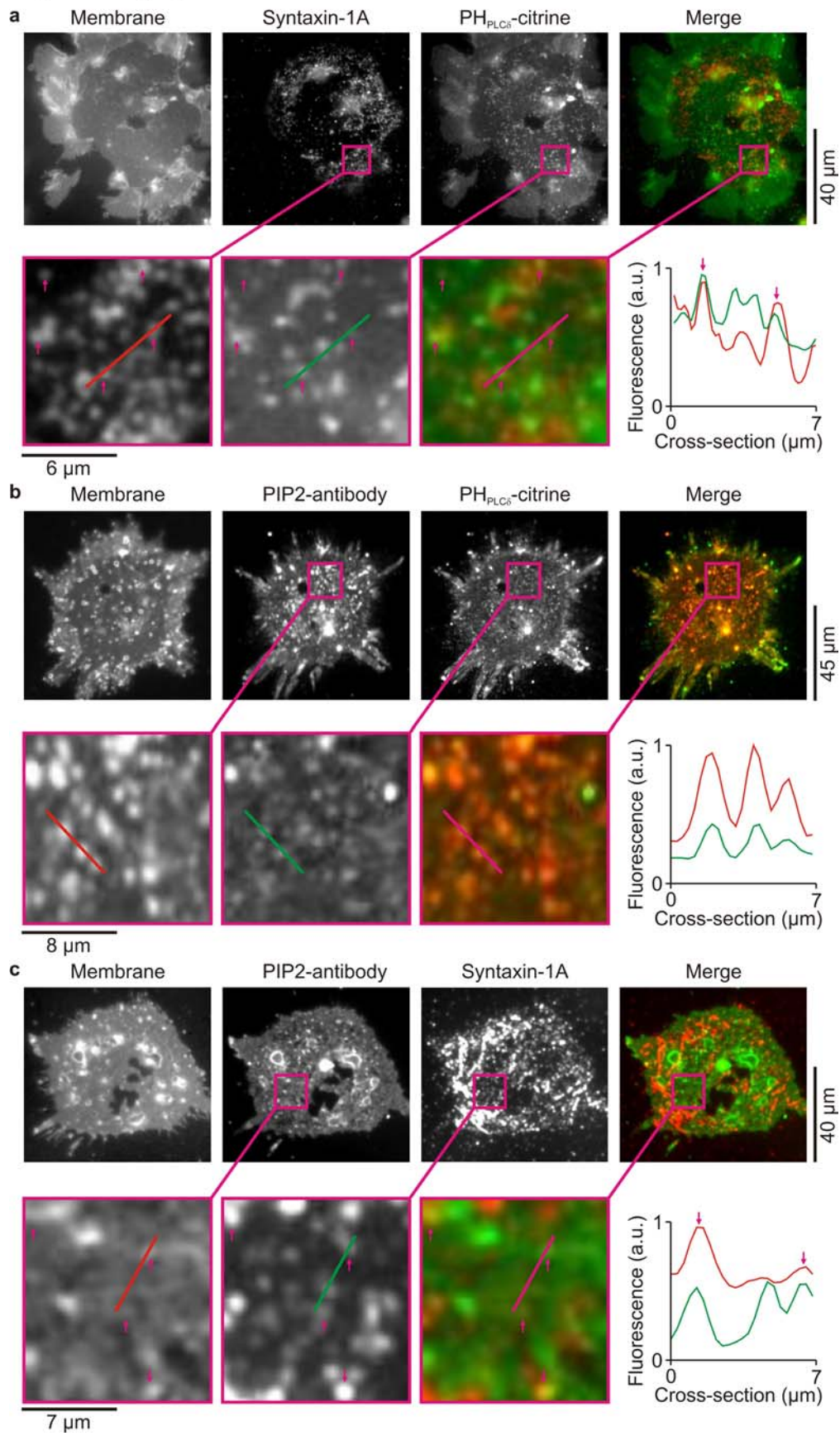
System setup of preassembled domains

In addition to spontaneous clustering, we also performed simulations at 310 K where the domains were preassembled and then relaxed in time. These systems contained 64 copies of syntaxin-1A$_{257-288}$ and 64 copies of PIP2 embedded in a 20 × 20 μm planar bilayer containing ~497 DOPC and 148 DOPS lipids (~20%). Moreover, the simulations contained ~21,000 solvent molecules and 150 mM NaCl. Similar to the simulations described above, additional Na$^+$ or Cl$^-$ counterions were added for charge neutralization and PIP2 was only present in the leaflet facing the *N*-terminal side of syntaxin-1A$_{257-288}$. The composition of such preassembled 64-sized syntaxin-1A$_{257-288}$ clusters was derived from the largest domains that were obtained in the spontaneous clustering simulations. We estimated a PIP2 to syntaxin molar ratio of 1:1, and less than 10% DOPC or DOPS for the composition of the bulk-phase of such domains. The rest of the PIP2 associated transiently to the periphery of the domains. We then performed simulations with corresponding syntaxin : PIP2 : DOPC : DOPS systems, that were coupled to their own periodic image to represent the 'bulk' phase of these domains. The stability of these systems was inferred from the area fluctuations and the remaining presence of heterogeneous mixing between PIP2, syntaxin-1A$_{257-288}$ and DOPC or DOPS. After equilibration, these domains were embedded in the bilayer by removing overlapping DOPC and DOPS. These domains were stable over the 6 μs simulated time. The domains were disrupted upon removal of the 5-phosphate of PIP2 (to PI3P, the reaction product of synaptojanin-1) or when both phosphates of PIP2 were removed.
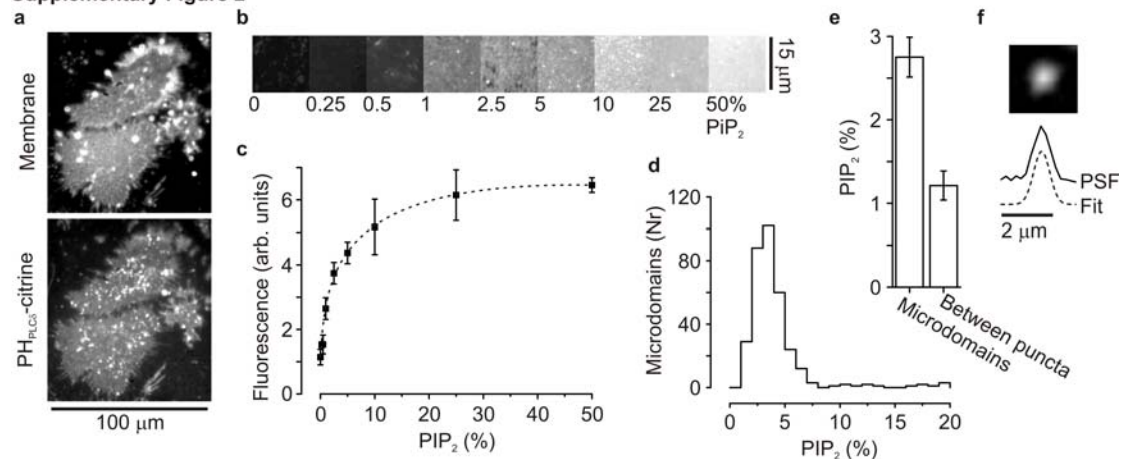
Cluster analysis

Domains were defined by a dynamic cluster algorithm. Here, syntaxin-1A$_{257-288}$ was considered to be part of a domain when the minimal distance to any of the other peptides was below 0.7 nm.

Supplementary Figure 1

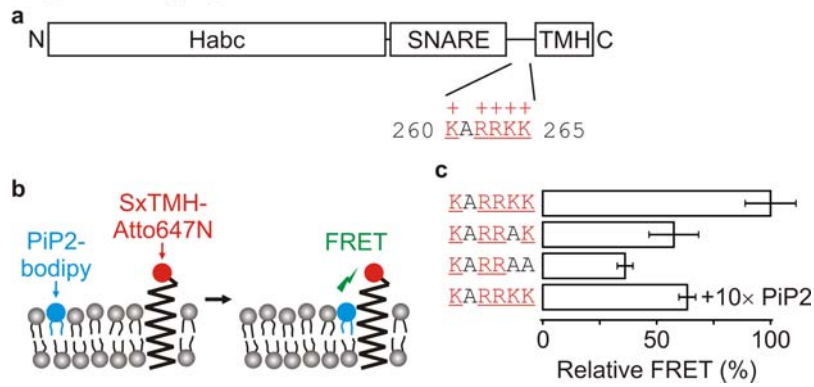**a** Membrane | Syntaxin-1A | PH$_{PLC\delta}$-citrine | Merge

40 µm

6 µm

Fluorescence (a.u.) | Cross-section (µm) | 0 ... 7

b Membrane | PIP2-antibody | PH$_{PLC\delta}$-citrine | Merge

45 µm

8 µm

Fluorescence (a.u.) | Cross-section (µm) | 0 ... 7

c Membrane | PIP2-antibody | Syntaxin-1A | Merge

40 µm

7 µm

Fluorescence (a.u.) | Cross-section (µm) | 0 ... 7

10

Supplementary Figure 1. Partial overlap of syntaxin-1A and PIP2 microdomains. (**a**) Plasma membrane sheets were prepared by removing the upper part of PC12 cells with a brief ultrasound pulse[3,9,12,24,45]. These membrane sheets were stained with the lipid probe TMA-DPH[32] (Membrane). Immunostaining with a monoclonal antibody raised against syntaxin-1A and a secondary antibody labeled with DyLight649 showed the clear clustering of syntaxin-1A in microdomains. These microdomains partially overlapped with the punctuate staining of $PH_{PLC\delta}$-citrine (pink arrows). The merged image and the cross-sections show syntaxin-1A in red and $PH_{PLC\delta}$-citrine in green. (**b**) Same as **a**, but now immunostained with a monoclonal antibody raised against PIP2 and a secondary antibody labeled with DyLight649. $PH_{PLC\delta}$-citrine (green) staining almost completely overlapped with that of the PIP2 antibody (red). (**c**) The overlap of syntaxin-1A and PIP2 microdomains with antibodies, similar to the study of Aoyagi *et al.*[2]. In this case, syntaxin-1A (green) was immunostained with a polyclonal antibody and a secondary antibody labeled with Cy5. PIP2 (red) was immunostained with a monoclonal PIP2-antibody as in **b** and with a secondary antibody labeled with Cy3. In both panels **a** and **c**, overlap of syntaxin-1A and PIP2 staining (*i.e.* with $PH_{PLC\delta}$-citrine or antibody) was present in 5–10% of all clusters. This value is substantially lower than reported previously with PIP2-antibodies[2] and this difference likely reflects heterogeneities in the PIP2 populations.
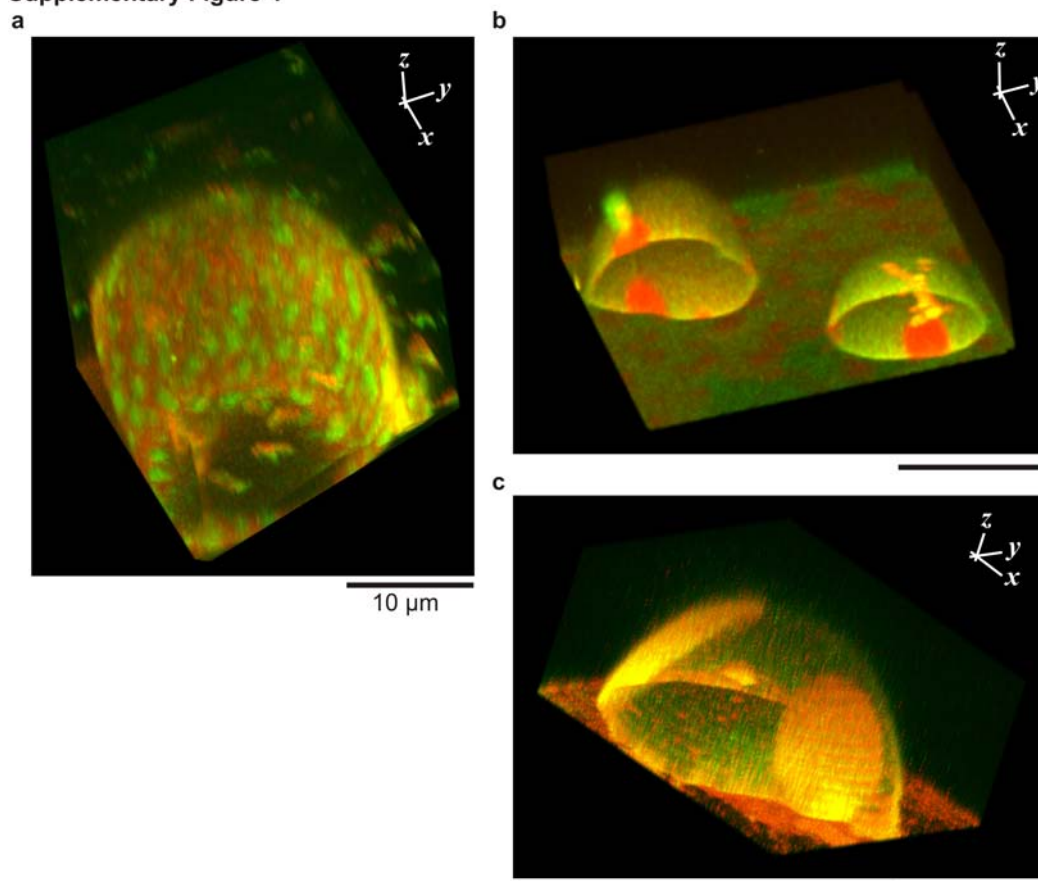
Supplementary Figure 2. Quantification of PIP2 in the diffraction limited microdomains, following the method of James *et al.*[9]. (**a**) Membrane sheets of PC12 cells stained with TMA-DPH[32] (upper panel) and $PH_{PLC\delta}$-citrine (lower). Note the punctuate staining of $PH_{PLC\delta}$-citrine. (**b**) Artificial supported bilayers of DOPC/PIP2 mixtures stained with $PH_{PLC\delta}$-citrine. (**c**) Quantification of the fluorescence intensity from **b**. (**d**) Distribution of the PIP2 surface concentrations in the microdomains. These surface concentrations were obtained by correlating the fluorescence intensity of the microdomains (from **a**) with that of the supported bilayers (from **b–c**). Panel **e** shows the average PIP2 concentration in the microdomains ($2.8 \pm 0.3\%$ (s.e.m.), $n = 305$ puncta from 25 sheets and 2 independent preparations) and inbetween the microdomains ($1.2 \pm 0.2\%$ (s.e.m.), $n = 25$ sheets). (**f**) Determination of the resolution of the fluorescent microscope by imaging of 0.2 μm-sized fluorescent beads. The intensity distributions (point spread functions; PSF) could be fitted with a Gaussian distribution with a variance of 445 nm (see Supp. Methods).
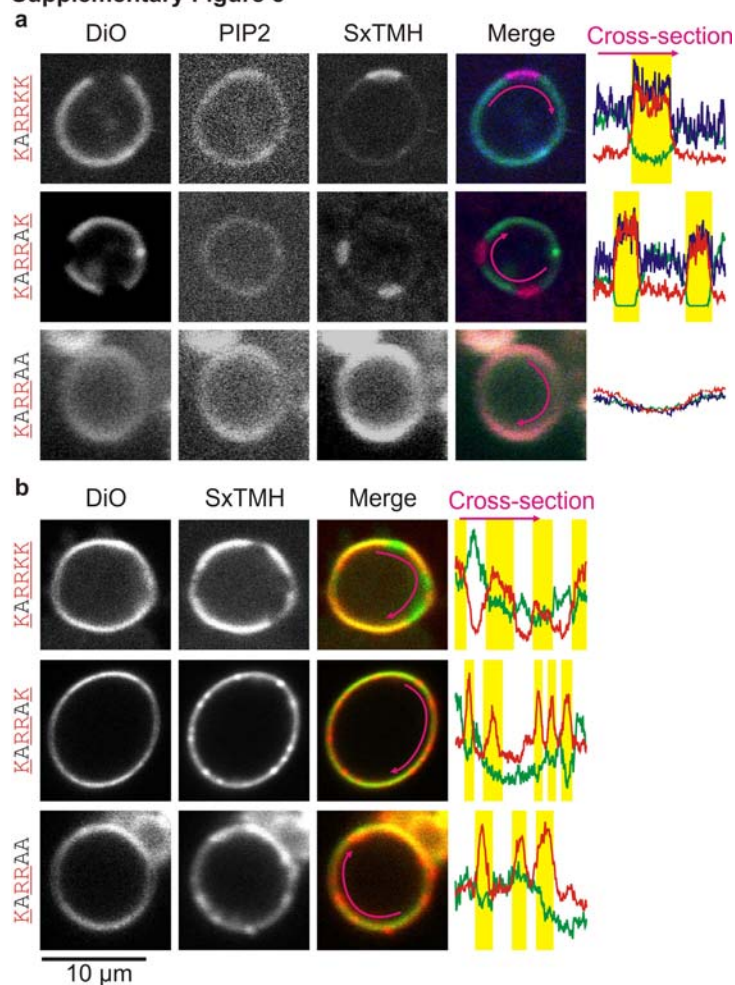
Supplementary Figure 3. The juxtamembrane polybasic stretch of syntaxin-1A interacts with PIP2. (**a**) Topology of syntaxin-1A showing the regulatory Habc domain, the SNARE-motif and the *C*-terminal transmembrane helix (TMH). The polybasic stretch (residues 260–265) that is located at the head-group layer of the membrane[15,16] is also indicated. (**b**) Scheme of a FRET experiment to show the interaction between the syntaxin-1A polybasic stretch and PIP2, similar to the assay by Murray and Tamm[17]. A synthetic peptide consisting of syntaxin-1A residues 257–288 (SxTMH) and *N*-terminally labeled with Atto647N was reconstituted in 100 nm-sized liposomes at 1:3,000 molar protein-to-lipid ratio. These liposomes were composed of a 4:1 molar ratio of DOPC/DOPS and contained 0.1% of bodipy-labeled PIP2 (bodipy-TMR-PI(4,5)P_2,C_{16}; Echelon Biosciences). Interaction results in FRET. (**c**) The sensitized emission (*i.e.* the acceptor fluorescence) relative to syntaxin-1A$_{257–288}$ with wild-type linker. Removal of charge from the linker decreased the FRET efficiency. FRET was also reduced when the liposomes contained 3 mol% unlabeled PIP2. Error bars; s.d. (*n* = 3).
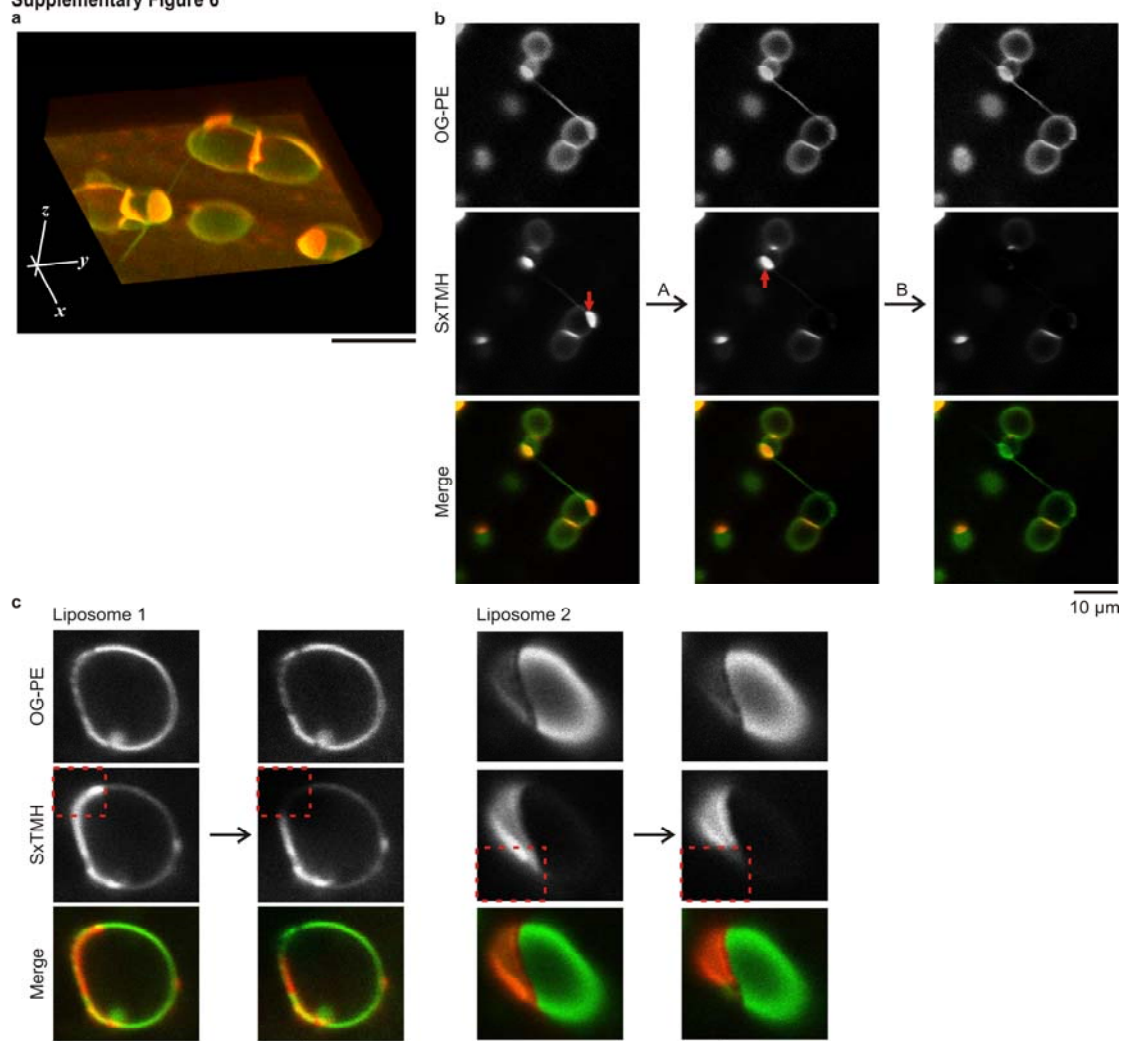
Supplementary Figure 4. 3D-reconstruction by confocal microscopy of syntaxin-1A domains in artificial membranes. (**a**) Cholesterol-excluded domains as predicted by Murray and Tamm[17]. Atto647N-labeled syntaxin-1A$_{257-288}$ (SxTMH; red) was reconstituted in GUVs and the membrane was labeled with 1.5 mol% DiO (green). The membrane was composed of a 4:1 molar ratio of DOPC and cholesterol. SxTMH clustered in many small domains. (**b**) Same as **a**, but now for PIP2-dependent domains. The membranes were composed of a 4:1 molar ratio of DOPC:DOPS with 1.5 mol% dioleoyl-PIP2 (1,2-dioleoyl-sn-glycero-3-phosphatidyl-(1'-myo-inositol-4',5'-bisphosphate)). SxTMH partitioned in one or two round 1–10 μm-sized domains (see also Fig. 2). (**c**) Same as **b**, but all fluorescent dyes have been changed to show that domain formation is independent of the dyes: Oregon green-DHPE (green) instead of DiO and rhodamine red (red) instead of Atto647N. A total of 1.5 mol% brain PIP2 was present instead of the dioleoyl-PIP2. Yellow indicates overlay of Oregon green-DHPE and SxTMH. Contrary to the positively charged DiO (panel **b**), the weakly anionic Oregon green-DHPE is not excluded from the domains. In **a–c**, the GUVs were attached to the coverslips. Free floating GUVs were also present, but 3D-microscopy was difficult because of movement.
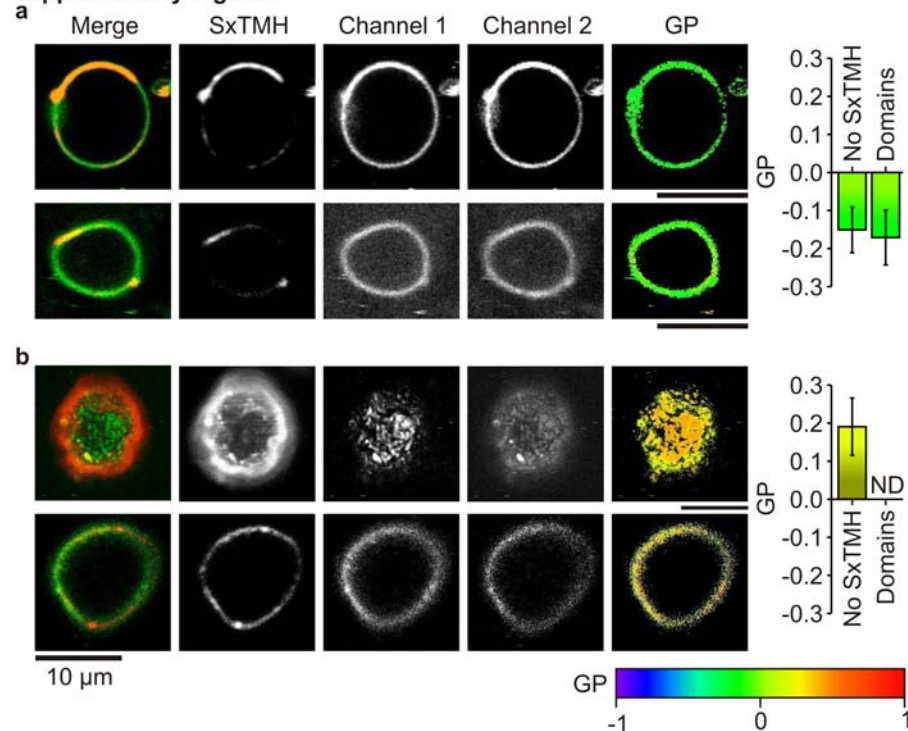
Supplementary Figure 5. Role of the polybasic linker region of syntaxin-1A in membrane clustering. (**a**) PIP2-domains. Syntaxin-1A$_{257-288}$ labeled with Atto647N (SxTMH; red) was reconstituted in GUVs (3 mol%). The membranes were composed of a 4:1 molar ratio of DOPC:DOPS with 1.2% PIP2. They were labeled with 1.5 mol% DiO (green) and 0.5 mol% bodipy-PIP2 (blue). Bodipy-PIP2 and SxTMH were 1.9 ± 0.2-fold (s.d., $n = 13$) and 5.5 ± 1.4-fold (s.d., $n = 27$) enriched in μm-sized domains based on fluorescence. However, these accumulations are lower estimates that are limited by the optics. No domains were observed when two positively charged residues were removed from the polybasic linker (K264A K265A; 260-KARRAA). (**b**) Cholesterol-dependent domains. Same as panel **a**, but now for membranes composed of a 4:1 molar ratio of DOPC:cholesterol. Here, SxTMH was 1.6 ± 0.2-fold (s.d., $n = 18$) enriched in many small domains. Contrary to the PIP2-domains from **a**, domains were still observed with the K264A K265A mutant. The pink arrows show the part of the membrane used for cross-sections. The yellow bars indicate the position of the domains.
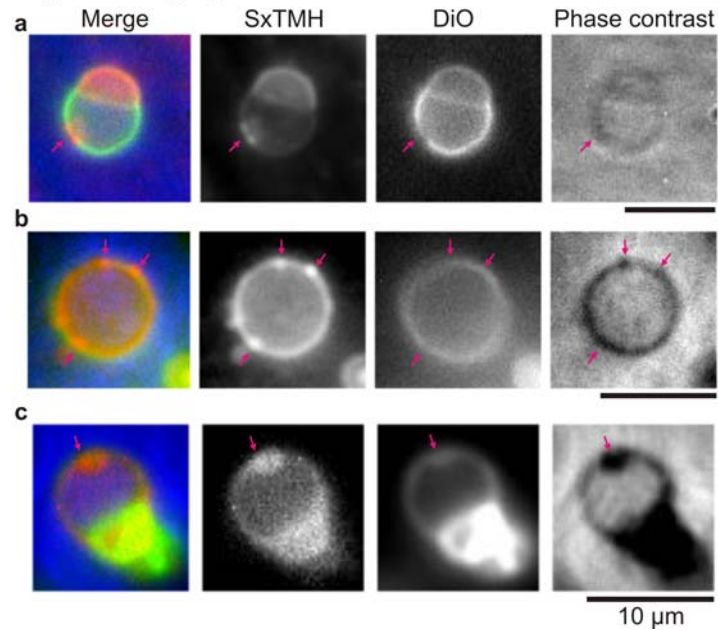
Supplementary Figure 6. Mobility of syntaxin-1A in the membrane domains. (**a**) PIP2-domains. 3D-reconstruction by confocal microscopy of PIP2-syntaxin-1A domains in artificial membranes. Rhodamine red-labeled syntaxin-1A$_{257-288}$ (SxTMH; red) was reconstituted in GUVs. The membranes were composed of a 4:1 molar ratio of DOPC:DOPS with 1.5 mol% PIP2 and were labeled with 1.5 mol% Oregon green-DHPE (OG-PE; green). PIP2 and SxTMH partitioned in μm-sized domains (see also Fig. 2). In this case, the GUVs were attached to the coverslip. Free floating GUVs were also present, but photobleaching and 3D-microscopy were difficult because of movement. (**b**) Photobleaching experiment where a high intensity red laser was focussed for ~5 s at the positions indicated by the arrows (step A and B). This resulted in photobleaching of rhodamine red-labeled syntaxin-1A$_{257-288}$ in the entire domain, indicating that it was mobile in these domains. Note that interestingly, the weakly anionic Oregon green-DHPE is not excluded from the PIP2-syntaxin-1A domains, whereas the positively charged DiO is excluded (Fig. 2, Supp. Fig. 4). (**c**) Same as **b**, but now for cholesterol-dependent clusters. Membranes contained a 4:1 molar ratio of DOPC:cholesterol and no PIP2. The red dashed square indicates the photobleached region. The left panels show a cross-section and the right panels a top-section of a GUV. Contrary to **b**, SxTMH was essentially immobile and fluorescence did not recover in 15 min in these cholesterol-dependent domains[17]. Similar experiments

show that components in cholesterol and sphingomyelin enriched domains ('rafts') are also essentially immobile[46].
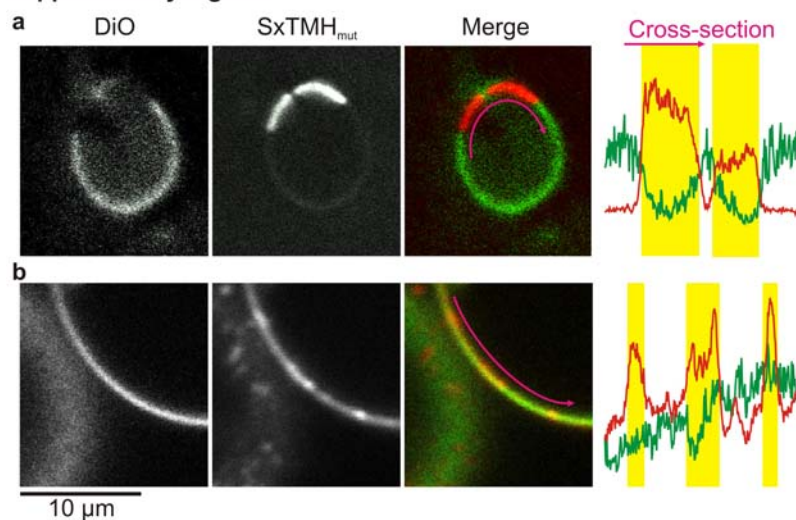
Supplementary Figure 7. Lipid packing probed with 6-dodecanoyl-2-dimethylaminonaphthalene (Laurdan). Laurdan inserts in the membrane and the wavelength of its emission is proportional to the hydration of the membrane[22,39]. Because the hydration of the membrane is directly related to the inter-lipid spacing, the emission of Laurdan can be used to determine lipid packing. Laurdan has two spectrally separated emission bands (low-λ: channel 1; high- λ: channel 2). The generalized polarization (GP) can be calculated from these values as a relative measure for membrane order. The GP can vary between -1 and 1 and a higher value means a denser lipid packing[22,39]. **(a)** PIP2-domains. Syntaxin-1A$_{257-288}$ labeled with Atto647N (SxTMH; red) was reconstituted in GUVs (3 mol%). The membranes were composed of a 4:1 molar ratio of DOPC:DOPS with 1.5% PIP2. The membranes were stained with 0.5–1% (total lipid) Laurdan. A GP value of -0.15 ± 0.06 (s.d., n = 6) for the membrane and -0.17 ± 0.7 (s.d., n = 6) for the domains was obtained. Both values are close to that of pure DOPC membranes[22] and indicative of highly hydrated (*i.e.* disordered) membranes. **(b)** In contrast, when the membranes were composed of a 4:1 molar ratio of DOPC:cholesterol (no PIP2) a GP value of 0.19 ± 0.07 (s.d., n = 5) was obtained. Cholesterol is known to result in denser lipid packing and to increase the GP value[22]. Interestingly, Laurdan did not partition in the cholesterol-induced SxTMH domains and we could not determine the GP value (N.D.). The upper row of panel **b** shows a top-section and the lower row a cross-section of a GUV. See Supp. Methods for details of the measurements.

Supplementary Figure 8. Phase contrast microscopy. (**a**) PIP2-domains. Syntaxin-1A$_{257-288}$ labeled with Atto647N (SxTMH; red; epi-fluorescence) was reconstituted in GUVs (3 mol%). The membranes were composed of a 4:1 molar ratio of DOPC:DOPS with 1.5% PIP2. They were labeled with 1.5 mol% DiO (green). Phase contrast microscopy (blue) showed no thickening of the membrane at the position of the domains (pink arrows). (**b**) Cholesterol-dependent domains as predicted by Murray and Tamm[17]. Same as **a**, but now for membranes composed of a 4:1 molar ratio of DOPC:cholesterol and no PIP2. In contrast to **a**, the membrane appeared darker in phase contrast microscopy at the position of the cholesterol-dependent SxTMH domains. (**c**) Artefact from condition **a**. Sometimes, the presence of PIP2 let to apparent thickening of the membrane. However, in these cases DiO was not excluded from the PIP2-domains. The thickening of the membrane by polycationic peptides has been reported before[47], and is likely caused by peptide-induced vesicle aggregation or spreading of a second on top of the first membrane. PIP2-domains that appeared thicker by phase contrast were excluded from the analysis. Phase contrast was measured with a Zeiss Plan-NEOFLUAR objective (100× 1.30 NA oil; Ph3).
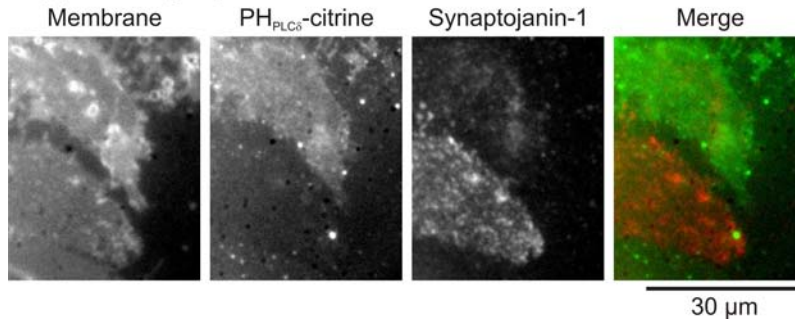
Supplementary Figure 9. Clustering of the dimerization mutant of syntaxin-1A. (**a**) PIP2-domains. Confocal cross-section of a GUV with 3 mol% of the M267A C271A I279A mutant of syntaxin-1A$_{257-288}$ (SxTMH$_{mut}$; red). This mutant prevents homodimerization of the transmembrane helix[23]. The membrane was composed of a 4:1 molar ratio of DOPC:DOPS with 1.5 mol% dioleoyl-PIP2 and was labeled with 1.5 mol% DiO (green). (**b**) Cholesterol-dependent domains as predicted by Murray and Tamm[17]. Same as **a**, but now for membranes composed of a 4:1 molar ratio of DOPC:cholesterol. In both **a** and **b**, SxTMH$_{mut}$ clustered in domains. We conclude that protein-protein interactions of the mutated transmembrane helix are still sufficient for both cholesterol and PIP2-dependent lateral sequestering (see also reference (24)). The pink arrows show the part of the membrane used for cross-sections. The yellow bars indicate the position of the domains.
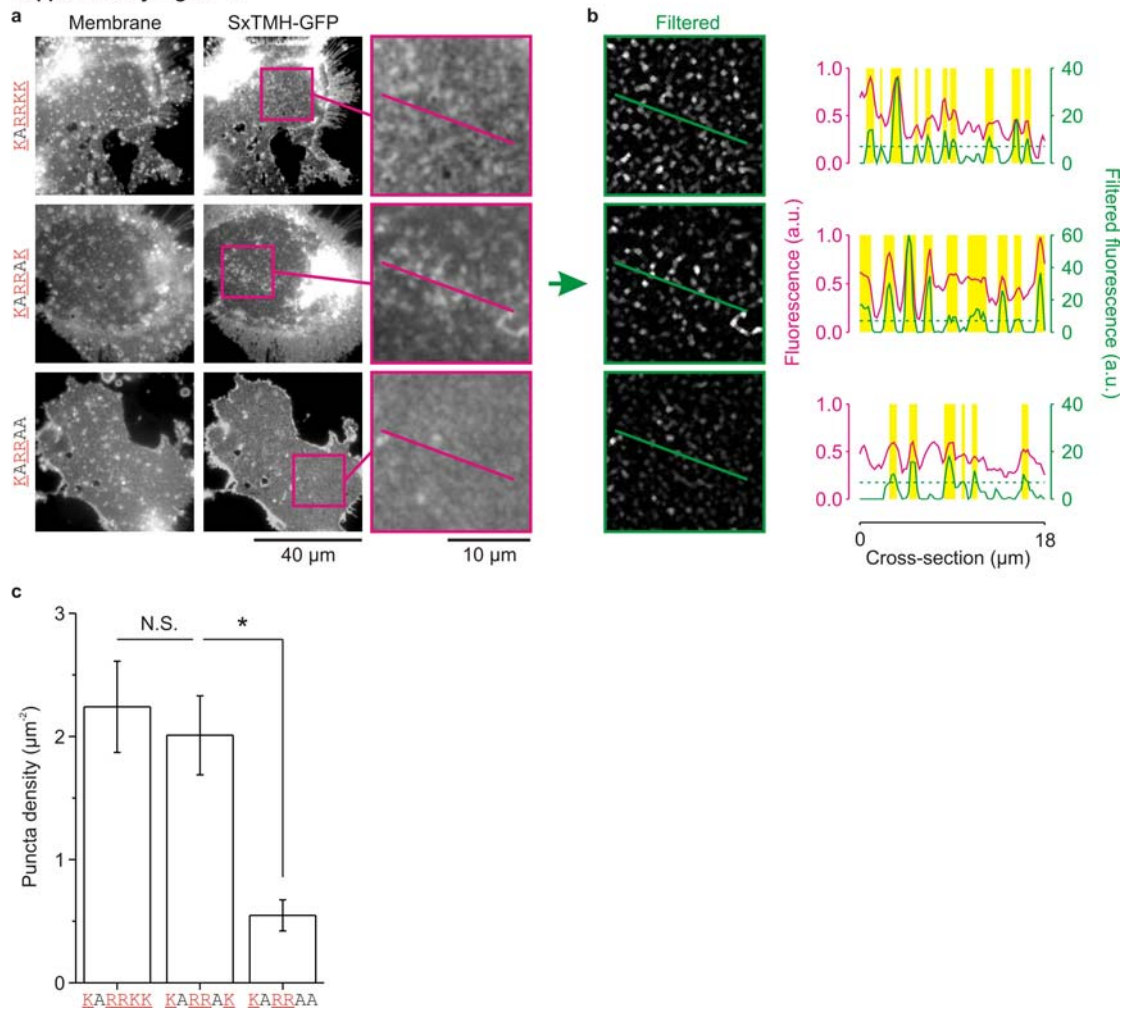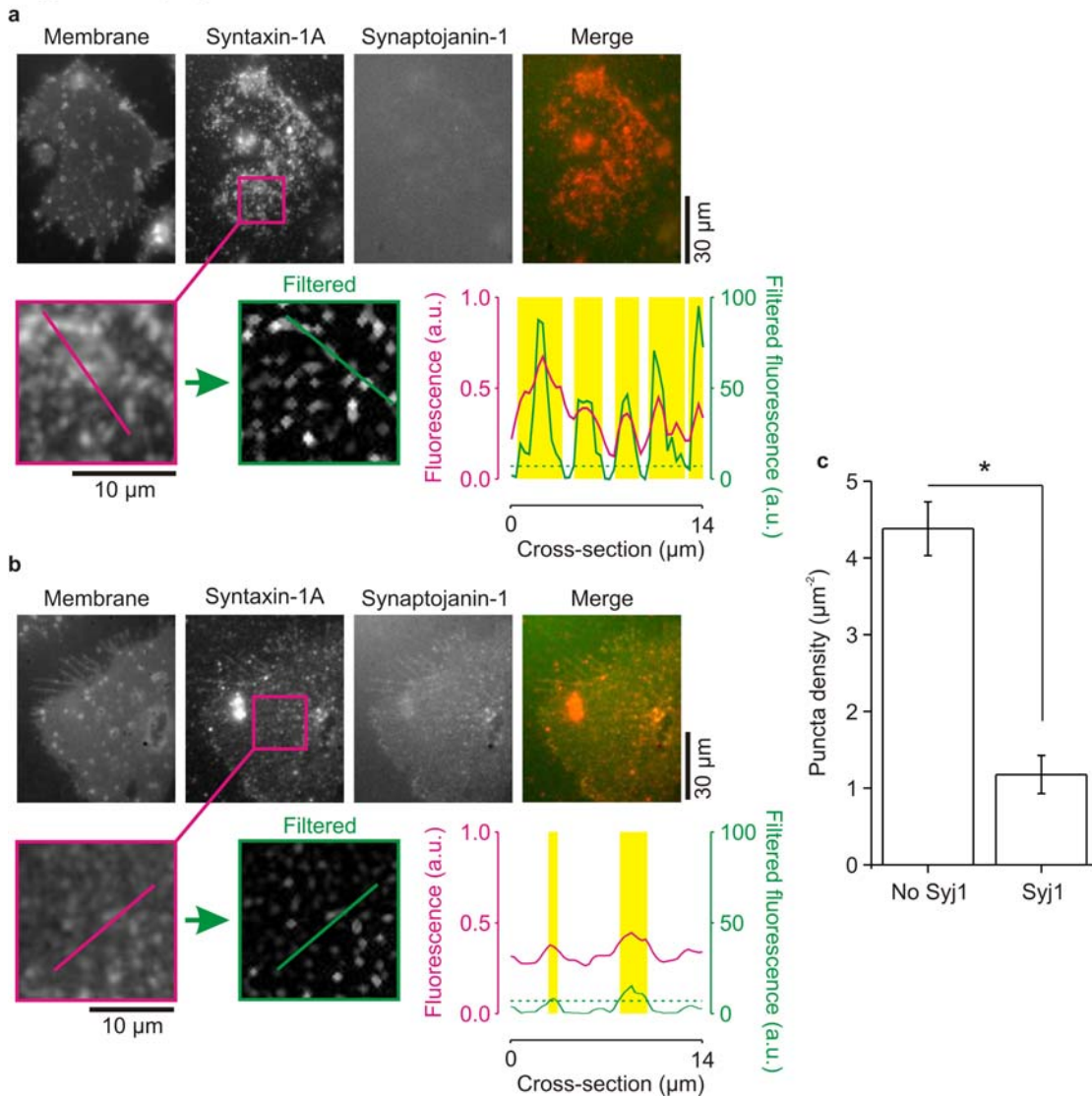
Supplementary Figure 10. Reduced membrane clustering of mutants in the juxtamembrane region of syntaxin-1A with membrane sheets. (**a**) Membrane sheets of PC12 cells expressing part of syntaxin-1A (residues 1–28 + 259–288) conjugated to monomeric enhanced GFP (SxTMH-GFP)[24]. Left panels: TMA-DPH[32] staining of the membranes. Middle: GFP fluorescence of the reporters. Right: magnification of the indicated region and cross-sections (pink). (**b**) To quantify the clustering of the GFP-reporter constructs, we processed the images with a granulometric filter[48]. This filter selects for grains of a certain size and can be used to process microscopy images with a heterogeneous background. The granulometric filtering assigns intensities by integral intensity thresholding[48]. The pink and green cross-sections show the fluorescence and the corresponding filtered intensities, respectively. We could hence determine the puncta above an arbitrary offset (at 7; dashed green curve). The yellow bars indicate the position of puncta above this offset. (**c**) Relative to wild-type (260-KARRKK, $n = 8$ from 2 independent samples), the K264A mutation (260-KARRAK, $n = 13$ from 2 independent samples) had no significant effect on clustering of the reporter (N.S.; $P = 0.7$, two-sided t test). In contrast, removal of two charges (K264A K265A; 260-KARRAA, $n = 18$ from 2 independent samples) reduced clustering 4-fold ($P = 3.4 \ 10^{-5}$, two-sided t test). Error bars show the standard error of the mean. See also supplementary figure 11.

Supplementary Figure 11. Reduced membrane clustering of mutants in the juxtamembrane region of syntaxin-1A with intact cells. (**a–c**) Same as supplementary figure 10, but now with TIRF microscopy on intact cells. Similar to the membrane sheets (Supp. Fig. 10), the K264A mutation (260-KARRAK, n = 8) had no significant (N.S.; P = 0.9, two-sided t test) effect on clustering of the reporter relative to wild-type (260-KARRKK, n = 8). In contrast, removal of two charges (K264A K265A; 260-KARRAA, n = 8) reduced clustering 8-fold (P = 2.2 10^{-3}, two-sided t test). Error bars show the standard error of the mean.
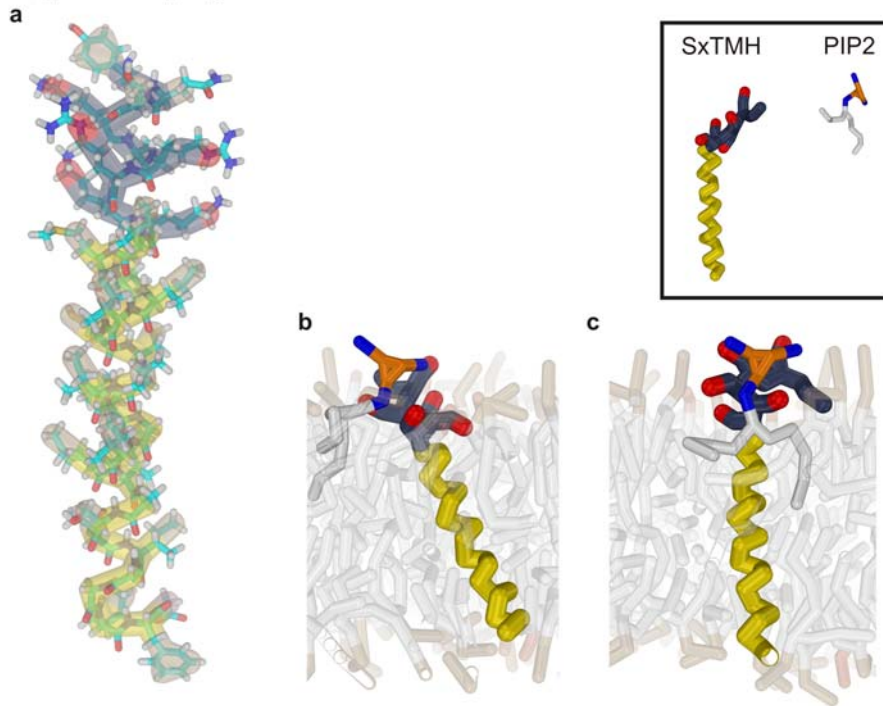
Supplementary Figure 12. Overexpression of synaptojanin-1 removes PIP2 from the plasma membrane. Membrane sheets of PC12 cells were stained with PH$_{PLC\delta}$-citrine. Overexpression of the RFP-tagged catalytic region of synaptojanin-1 (residues 498–901) fused to a CAAX-box (for membrane-targeting)[7,49] completely blocked PH$_{PLC\delta}$-citrine binding, as reported previously[7]. Synaptojanin-1 is the 5-phosphatase of PIP2[6,7].
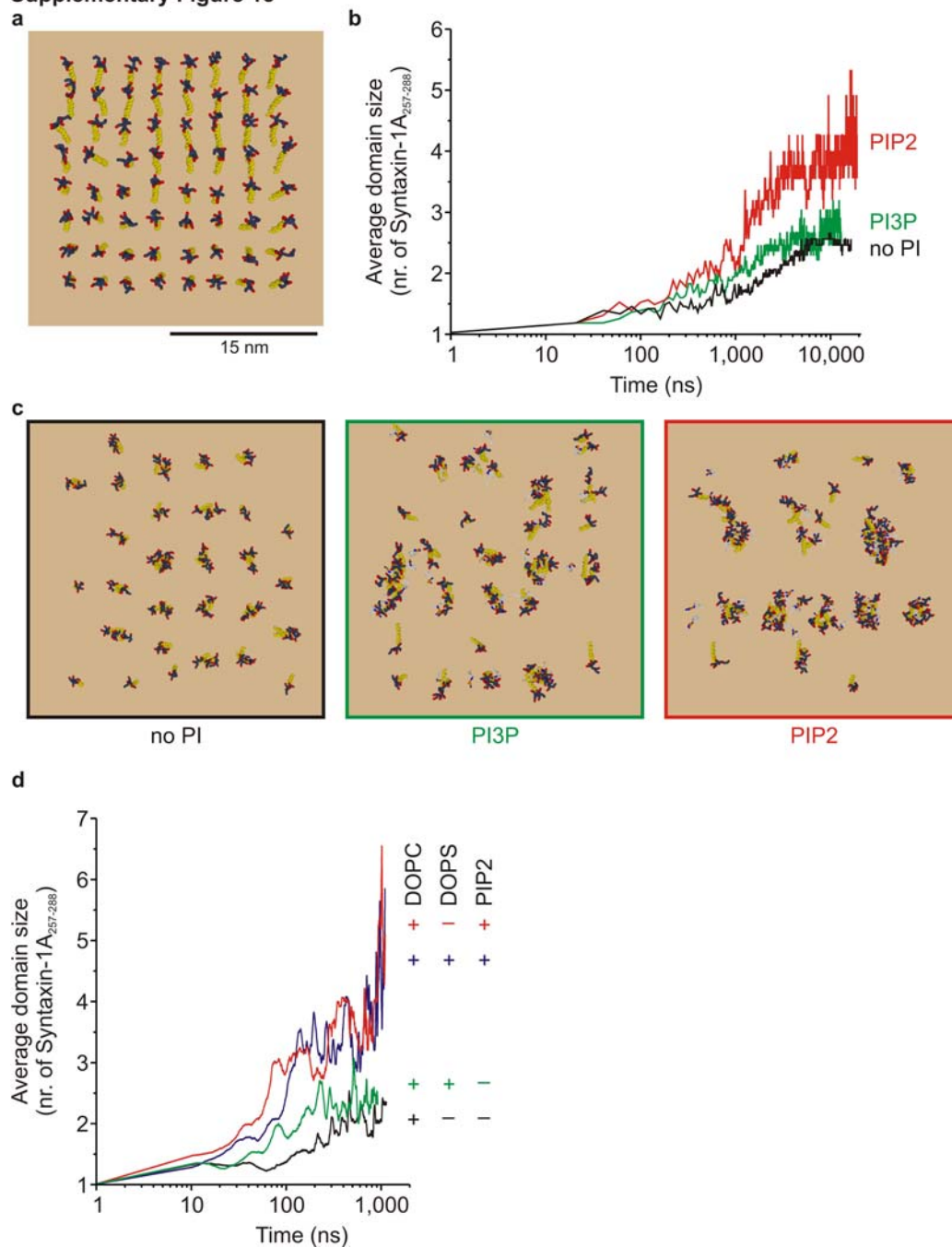
Supplementary Figure 13. Removal of PIP2 reduces syntaxin-1A clustering in PC12 cells (see also Fig. 3). (**a**) Membrane sheet of a PC12 cell not expressing the synaptojanin-1-RFP construct (green). The membrane was stained with TMA-DPH[32]. Immunostaining with the monoclonal antibody HPC-1 raised against syntaxin-1A[31] and a secondary antibody labeled with DyLight649 showed that endogenous syntaxin-1A clustered in microdomains (red). To quantify the clustering of syntaxin-1A, we processed the images with the granulometric filter[48] also used in Supp. Fig. 10–11. The pink and green cross-sections show the fluorescence and the corresponding filtered intensities, respectively. The yellow bars indicate the position of the puncta above an arbitrary offset (at 7; dashed green line; see also Supp. Fig. 10–11). (**b**) Same as **a**, but now for a cell overexpressing the RFP-tagged and membrane-targeted catalytic region of synaptojanin-1 (residues 498–901)[7,49]. (**c**) The density of puncta above the offset from panels **a** and **b**. Relative to wild-type ($n = 16$ from 2 independent samples), overexpressing synaptojanin-1 ($n = 12$ from 2 independent samples) reduced clustering 3.7-fold ($P = 2.2 \times 10^{-7}$, two-sided t test). Error bars show the standard error of the mean.

Supplementary Figure 14. Simulations of the syntaxin-1A – PIP2 interactions. (**a**) Overlap of the coarse-grained model for the syntaxin-1A$_{257-288}$ peptide (SxTMH) with the crystal structure (light blue; protein data bank 3HD7)[50]. (**b–c**) Snapshots of SxTMH interactions with PIP2. We simulated SxTMH both with a (**b**) structured (α-helical) and (**c**) unstructured linker (residues 257–265). Orange-blue: anionic PIP2 headgroup (charges in blue). White: alkyl chains of PIP2. Yellow: transmembrane region of syntaxin-1A$_{257-288}$ (residues 266–288). Blue-red: polybasic linker region (residues 257–265, charges in red).

Supplementary Figure 15. Coarse-grained molecular dynamics simulation of spontaneous domain assembly. (**a**) Top view on the membrane. 64 copies of syntaxin-1A$_{257-288}$ were embedded in a DOPC membrane. The membranes contained 40 copies of PIP2 (red), PI3P (green), or no phosphoinositides (black; no PI). Yellow: transmembrane helix of syntaxin-1A$_{257-288}$ (residues 266–288). Blue-red: polybasic linker region (residues 257–265, charges in red). (**b**) The average size of the syntaxin-1A$_{257-288}$ clusters is plotted over the simulation time. Syntaxin-1A$_{257-288}$ strongly clustered when PIP2 was present, whereas in the other cases predominantly dimer formation was observed and no/weak clustering. (**c**) Snapshots at the end of the simulations from **b** showing the apparent clustering. (**d**) The effect of monovalent lipids on spontaneous domain assembly. Same as panel **b**, but now 16 copies of

syntaxin-1A$_{257–288}$ were incorporated into membranes (~500 lipids total) of various compositions and in presence of 150 mM NaCl. Black: pure DOPC. Green: DOPC + 20% DOPS. Red: DOPC + 25 copies of PIP2. Blue: DOPC + 20% DOPS + 25 copies of PIP2.

Legend to Supplementary Movie 1. Simulation of the dynamic and amorphous PIP2-syntaxin-1A microdomains. The movie shows a 1 µs time-course of the simulation from figure 4. Note the relatively high mobility of syntaxin-1A$_{257-288}$ and PIP2 within the domain. See figure 4 and the supplementary materials for details.

Supplementary references

30. Várnai, P. & Balla, T. Visualization of phosphoinositides that bind pleckstrin homology domains: calcium- and agonist-induced dynamic changes and relationship to myo-[3H]inositol-labeled phosphoinositide pools. *J. Cell Biol.* **143,** 501-510 (1998).

31. Barnstable, C.J., Hofstein, R. & Akagawa, K. A marker of early amacrine cell development in rat retina. *Brain Res.* **352,** 286-290 (1985).

32. Illinger, D., *et al.* A comparison of the fluorescence properties of TMA-DPH as a probe for plasma membrane and for endocytic membrane. *Biochim. Biophys. Acta.* **1239,** 58-66 (1995).

33. Nägerl, U.V., Willig, K.I., Hein, B., Hell, S.W. & Bonhoeffer, T. Live-cell imaging of dendritic spines by STED microscopy. *Proc. Natl. Acad. Sci. USA* **105,** 18982-18987 (2008).

34. Hein, B., Willig, K.I., Wurm, C.A., Westphal, V., Jakobs, S. & Hell, S.W. Stimulated emission depletion nanoscopy of living cells using SNAP-tag fusion proteins. *Biophys. J.* **8,** 158-163 (2010).

35. Chakraborty, M., Chowdhury, D. & Chattopadhyay, A. Spin-coating of polystyrene thin films as an advanced undergraduate experiment. *J. Chem. Educ.* **80,** 806-809 (2003).

36. Mennicke, U. & Salditt, T. Preparation of solid-supported lipid bilayers by spin-coating. *Langmuir* **18,** 8172-8177 (2002).

37. Langosch, D. *et al.* Peptide mimics of SNARE transmembrane segments drive membrane fusion depending on their conformational plasticity. *J. Mol. Biol.* **311**, 709-721 (2001).

38. Doeven, M.K. *et al.* Distribution, lateral mobility and function of membrane proteins incorporated into giant unilamellar vesicles. *Biophys. J.* **88**, 1134-1142 (2005).

39. Gaus, K., Zech, T. & Harder, T. Visualizing membrane microdomains by Laurdan 2-photon microscopy. *Mol. Membr. Biol.* **23,** 41-48 (2006).

40. Hess, B., Kutzner, C., van der Spoel, D. & Lindahl. E. GROMACS 4: algorithms for highly efficient, load-balanced, and scalable molecular simulation. *J. Chem. Theory Comput.* **4,** 435-447 (2008).

41. Monticelli, L. *et al*. The MARTINI coarse-grained force field: extension to proteins. *J. Chem. Theory Comput.* **4,** 819-834 (2008).

42. Berendsen, H.J.C., Postma, J.P.M., van Gunsteren, W.F., Dinola, A. & Haak. J.R. Molecular dynamics with coupling to an external bath. *J. Chem. Phys.* **81,** 3684-3690 (1984).

43. Marrink, S.J., Periole, X., Tieleman, D.P. & de Vries. A.H. Comment on "On using a too large integration time step in molecular dynamics simulations of coarse-grained molecular models". *Phys. Chem. Chem. Phys.* **12,** 2254-2256 (2010).

44. Lopez, C.A. *et al*. The Martini coarse grained force field: extension to carbohydrates. *J. Chem. Theory Comput.* **5,** 3195-3210 (2009).

45. Zilly, F.E. *et al.* Ca(2+) induces clustering of membrane proteins in the plasma membrane via electrostatic interactions. *EMBO J.* **30,** 1209-1220 (2011).

46. Kahya, N., Scherfeld, D., Bacia, K., Poolman, B. & Schwille, P. Probing lipid mobility of raft-exhibiting model membranes by fluorescence correlation spectroscopy. *J. Biol. Chem.* **278,** 28109-28115 (2003).

47. Murray, D., *et al.* Electrostatic properties of membranes containing acidic lipids and adsorbed basic peptides: theory and experiment. *Biophys. J.* **77,** 3176-3188 (1999).

48. Prodanov, D., Heeroma, J. & Marani, E. Automatic morphometry of synaptic boutons of cultured cells using granulometric analysis of digital images. *J. Neurosci. Methods* **151,** 168-177 (2006).

49. Krauss, M. *et al.* ARF6 stimulates clathrin/AP-2 recruitment to synaptic membranes by activating phosphatidylinositol phosphate kinase type Igamma. *J. Cell Biol.* **162,** 113-124 (2003).

50. Stein, A., Weber, G., Wahl, M.C. & Jahn, R. Helical extension of the neuronal SNARE complex into the membrane. *Nature* **460,** 525-528 (2009).